JOURNAL OF THERMOPHYSICS AND HEAT TRANSFER
Vol. 14, No. 3, July–September 2000

Effects of Heat Source Arrangements on Marangoni Convection in Electrostatically Levitated Droplets

S. P. Song,* P. Dailey,† and B. Q. Li‡
Washington State University, Pullman, Washington 99164

A numerical study is presented of surface deformation, Marangoni convection, and temperature distribution in an electrostatically levitated melt droplet under both terrestrial and microgravity conditions. The numerical model is developed based on the boundary element solution of the electric field distribution outside the droplet, which is then integrated with the weighted residuals method for determining the droplet shapes that are defined by the balance of the electrostatic stresses, surface tension, and hydrostatic pressure when gravity is present. The internal fluid flow and temperature distribution in the electrostatically deformed droplet are computed using the finite element method. Computed results show that the electrostatic normal stresses induced by the applied electric field deform the droplet by pulling at its two poles. Noticeable Marangoni convection results from all laser heat source arrangements studied. Among these arrangements, the ring heat source produces the lowest velocity level and the smallest temperature gradient, whereas the highest velocity and greatest temperature difference occur when heating is applied at only one of the poles. For all cases, an increase in the droplet surface covered by the laser beam helps to reduce the temperature difference and hence thermally induced flows in the droplet.

Nomenclature

a	= radius
C, C_p	= geometric coefficient, heat capacity
E	= applied electric field
$\boldsymbol{g}$, G	= gravity constant, Green's function for free space
$\hat{i}$, $\hat{j}$	= unit vector of the ith and jth component
k	= thermal conductivity
$\boldsymbol{n}(n_r, n_z)$	= outward normal, its r and z components
Q	= net charge on the droplet
Q_0	= laser beam heat flux constant
R	= distance measured from the center of the unformed droplet
s	= dummy variable for surface integral
T, T_∞, T_r	= temperature, temperature of surroundings, reference temperature
$T_{\max}$, $T_{\min}$	= maximum and minimum temperatures
$\boldsymbol{t}$	= tangential vector
$U_{\max}$	= maximum velocity
$\boldsymbol{u}$, $\boldsymbol{U}$	= velocity, velocity at discretized nodal points
$\hat{z}$, z	= unit vector of z direction, z coordinate
β	= thermal expansion coefficient
γ	= surface tension
ΔT	= difference between $T_{\max}$ and $T_{\min}$
δ_{ij}	= delta function: $\delta_{ij} = 1$ when $i = j$; $\delta_{ij} = 0$ when $i \neq j$
ε	= emissivity
ε_0	= permittivity of free space region designated Ω_2
η	= molecular viscosity
θ	= θ direction
ρ	= density
σ_e, σ_s	= surface charge distribution, Stefan–Boltzmann constant
$\bar{\sigma}$	= stress tensor including electric pressure
Φ	= electric potential
ϕ, φ, ψ	= shape functions for velocity, temperature, and pressure
Ω	= computational domain
∇	= gradient operator

Subscripts

d	= droplet
i	= ith point
l	= laser beam
1, 2	= region inside and outside the droplet

Superscripts

i, j	= ith and jth components
T	= transpose

I. Introduction

WHEN a sample, solid or liquid, is charged positively and placed in a static electric field pointing upward, the Coulomb force is generated in the same direction of the electric field and acts on the sample as a result of interaction between the impressed charges and the applied electric field. If either the electric field or the applied charge is large enough, the Coulomb force can be sufficiently strong to balance the weight of the sample. As a consequence, the charged sample is levitated against gravity. This well-known principle of electrostatics is the foundation upon which the electrostatic levitation technology is developed. Simple as it may seem, levitation in an electric field requires a quite delicate feedback control mechanism to ensure stabilized levitation of a charged sample (Refs. 1 and 2; W. K. Rhim, Jet Propulsion Laboratory, California Institute of Technology, personal communication, 1997).

Originally developed under terrestrial conditions, electrostatic levitation is now being explored for microgravity applications. Because gravity is negligible in space vehicles, the concept of levitation by the electric forces is exploited to position the sample at a designated location and to prevent it from drifting around in microgravity environment. Levitated droplets have several very important applications. First, a levitated droplet may be cooled far below its melting point (i.e., at a large undercooling stage) without being subject to the container wall-induced nucleation, thereby providing a unique vehicle for the experimental verification of the fundamental theory governing solidification phenomena, such as homogeneous nucleation and grain growth in undercooled melts. Also, electrostatic levitation can be applied to determine the thermophysical properties of various materials, in particular, those that are of a high melting point and

Received 12 November 1998; revision received 30 December 1999; accepted for publication 7 January 2000.

*Graduate Student, School of Mechanical Engineering; currently at Ford Motor Co., Dearborn, MI 48123.
†Senior Student, School of Mechanical Engineering.
‡Associate Professor, School of Mechanical Engineering; li@mme.wsu.edu.

corrosive in nature, and also those at the undercooled stage, without contamination resulting from container walls. Moreover, levitated droplets allow better control of protein crystal growth from solutions and hold promise for processing materials of ultrahigh purity. These attractive features have been the major impetus for an internationally consorted effort to develop and construct an electrostatic levitation device and install it permanently in the much publicized International Space Station, which is under construction.

Electric fields have some advantages over other types of fields such as magnetic fields, for levitation purposes. Perhaps one of the most important advantages is that electrostatic levitation in principle can support any type of material including metals, semiconductors, and insulators, while magnetic levitation is limited to electrical conductors. Also, for electrically conducting samples levitated in vacuum, no internal convection results from the electric stresses, since the whole droplet is at an equal potential and the Maxwell stress inside the sample is uniform. This is extremely important for some planned microgravity experiments to measure certain thermophysical properties, such as melt viscosity and surface tension by induced droplet oscillation in microgravity, because a strong flow can make it very difficult to interpret the experimental measurements accurately.[3–5]

There appears to have been very limited literature devoted to the internal convection and heat transfer aspects of the droplets levitated in electric fields. The published work on electrostatic levitation is concerned primarily with system design and control.[2] There also have been some analyses on an inviscid oscillation of charged droplets for simple electric field configuration and shape stability.[6–8] Information on electromagnetic and transport phenomena in electrostatically levitated droplets is very scarce, however, despite the growing importance of electrostatic levitation in the microgravity research community. An exception is the work by Sadhal et al., who derived analytical expressions for the temperature and internal flow in a liquid sphere under the assumption of pure thermal and momentum diffusion.[9] Drop shape deformation induced by electric fields, however, was not considered. Experience with earthbound electrostatic levitation has suggested that internal fluid flow may develop in levitated droplets. Whereas electrostatic forces are not responsible for an internal flow in a conducting sample, it can arise from other sources. For example, under terrestrial conditions, natural convection occurs due to a temperature difference in the droplet. In addition, Marangoni convection may be induced in a levitated droplet when its surface tension varies with temperature.[2,10] These thermally induced flows are sensitive to the heat source arrangements used for droplet heating, which vary depending on the specific system design or experiment. Knowledge of heat source effects on the internal flow is of critical importance for an accurate interpretation of the experimental measurements obtained from the levitated droplet, for levitation system development, and for a fundamental understanding of the droplet behavior.

This paper describes a numerical study of surface deformation, fluid flow, and thermal phenomena associated with an electrostatically levitated droplet, focusing on the effects of heating source arrangements on the Marangoni convection and temperature distributions. The motivation for the work is derived from the need to develop a good understanding as well as first principal estimates of electrostatically induced surface deformation and temperature and internal fluid flowfields in these levitated droplets. The information should be of great value in establishing a rational basis for developing electrostatic levitation systems for space applications as well as for planning relevant experiments in space shuttle flights or in the upcoming International Space Station. For this purpose, first principal numerical models are developed to predict the thermal and fluid flowfields and electrostatically induced deformation of the droplets levitated in electrostatic fields. The computational methodology entails the mixed use of boundary element and finite element methods. The boundary element method is employed to obtain the solution for the electrostatic field, which is then coupled with the weighted residuals method for an iterative solution of the equilibrium free surface shapes of the levitated droplets. The temperature distribution and fluid flowfield in the droplets are calculated using the finite element method. Numerical calculations are performed to obtain information on both the steady-state and the transient evolution of thermal and fluid flowfields in the levitated droplets for various heating arrangements that either have been applied or are being considered for electrostatic levitation. The transient results are useful for assessing the behavior of the levitated droplets as they are cooled into undercooling regions. Both microgravity and terrestrial conditions are considered; the latter is useful for ground-based testing of electrostatic levitation processes.

II. Mathematical Formulation

The problem under consideration is illustrated in Fig. 1. An electrically conducting liquid droplet, charged positively, is suspended in an electrostatic field generated by two horizontal, parallel electrodes placed far apart (Fig. 1a). Two laser beams are applied in the areas around the north and south poles to melt the sample and/or heat it up to a designated temperature (Fig. 1b). The droplet shapes are defined by the balance of the local forces acting along the free surfaces, which include the electric stresses and the surface tension forces. The electric stresses can be computed when the electric field distribution along the droplet surface is known. To obtain the field distribution, the Maxwell equations need to be solved. For the present problem the equations simplify to a partial differential equation involving the electric potential only.[10] For an electrically conducting droplet such as a molten silicon or metal droplet, only the electric potential outside the droplet is needed, since the electric field inside the droplet is identically zero by the Gauss law.[6] Thus, the equations governing the electric potential distribution in the region outside the droplet can be written as follows[11]:

$$\nabla^2\Phi = 0, \qquad \in\Omega_2 \tag{1}$$

$$\Phi = \Phi_0, \qquad \in\Omega_1 \cap \Omega_2 \tag{2}$$

$$\varepsilon_2 \boldsymbol{n}\cdot\nabla\Phi = -\sigma_e, \qquad \in\Omega_1 \cap \Omega_2 \tag{3}$$

$$\oiint_{\partial\Omega_1} \sigma_e \,\mathrm{d}s = -\oiint_{\partial\Omega_1} \varepsilon_0 \boldsymbol{n}\cdot\nabla\Phi \,\mathrm{d}s = Q, \qquad \in\Omega_1 \cap \Omega_2 \tag{4}$$

$$\Phi = -ER\cos\theta, \qquad R \to \infty \tag{5}$$

with Φ_0 being the unknown constant potential of the surface of the droplet, which is calculated by the surface integral representing charge conservation, as expressed in Eq. (4).

As discussed in the Sec. I, the internal convection in an electrically conducting liquid droplet is attributed to thermal effects only, which

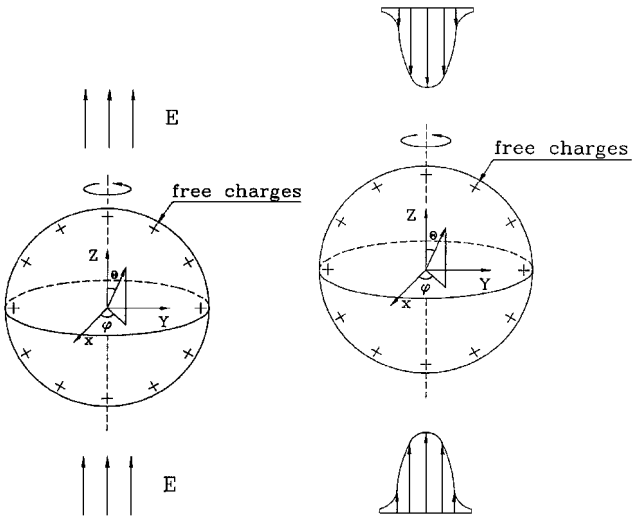

a) Levitation mechanism **b) Laser heating arrangement**

Fig. 1 Schematic representation of a positively charged melt droplet levitated in an electrostatic field.

in turn are determined by laser heating and radiative heat loss to the environment. The mathematical description of the fluid flow and temperature distribution in the melt droplet electrostatically levitated in microgravity is given by the Navier–Stokes equation and the thermal energy balance equation, viz.,

$$\nabla \cdot \boldsymbol{u} = 0, \qquad \in \Omega_1 \tag{6}$$

$$\rho \frac{\partial \boldsymbol{u}}{\partial t} + \rho \boldsymbol{u} \cdot \nabla \boldsymbol{u} = -\nabla p + \nabla \cdot \eta[\nabla \boldsymbol{u} + (\nabla \boldsymbol{u})^T] - \rho \beta \boldsymbol{g}(T - T_r) \qquad \in \Omega_1 \tag{7}$$

$$\rho C_p \frac{\partial T}{\partial t} + \rho C_p \boldsymbol{u} \cdot \nabla T = \nabla \cdot k \nabla T, \qquad \in \Omega_1 \tag{8}$$

These fluid flow and heat transfer equations may be solved subject to both thermal and mechanical boundary conditions. Across a free surface, the normal velocity must obey the kinematic condition and mechanical stresses must be continuous. These, along with the thermal environment given in Fig. 1b, are formulated mathematically and stated as follows:

$$-k\boldsymbol{n} \cdot \nabla T = \varepsilon \sigma_s \left(T^4 - T_\infty^4\right) - Q_0 e^{-r_l^2/a_l^2}, \qquad \in \Omega_1 \cap \Omega_2 \tag{9}$$

$$\boldsymbol{u} \cdot \boldsymbol{n} = 0, \qquad \in \Omega_1 \cap \Omega_2 \tag{10}$$

$$\boldsymbol{n} \cdot \bar{\sigma} \cdot \boldsymbol{n} = 2\gamma H, \qquad \in \Omega_1 \cap \Omega_2 \tag{11}$$

$$\boldsymbol{t} \cdot \bar{\sigma} \cdot \boldsymbol{n} = \frac{\mathrm{d}\gamma}{\mathrm{d}T} \boldsymbol{t} \cdot \nabla T, \qquad \in \Omega_1 \cap \Omega_2 \tag{12}$$

Clearly, the last equation represents the flow along the surface of the droplet induced by surface tension force if it is a function of temperature.

III. Methods of Solution

The preceding equations, along with the boundary conditions, are solved by the boundary element and finite element methods. Computer programs were developed for the calculations. Because the numerical details including program structure and accuracy of calculations are documented in other related publications,[12–14] only a brief outline is given here.

The scalar equation describing the electric potential distribution is solved by the boundary element method. The method is uniquely suitable for the solution of these types of problems and is superior over domain-based methods such as the finite element and finite difference methods. This is because the present problem involves a boundary at infinity, and as such, domain-based methods would require the discretization of the entire free space outside the droplet. In contrast, the boundary element method automatically incorporates the boundary conditions at infinity directly into the integral formulation[13]:

$$C_i \Phi_i + \int_{\partial\Omega} \Phi \frac{\partial G}{\partial n} \mathrm{d}\Gamma = \int_{\partial\Omega} \frac{\partial \Phi}{\partial n} G \, \mathrm{d}\Gamma + \int_{\partial\Omega} En_z G \, \mathrm{d}\Gamma - \int_{\partial\Omega} Ez \frac{\partial G}{\partial n} \mathrm{d}\Gamma - C_i Ez_i \tag{13}$$

where $\partial\Omega$ designates the surface of the droplet. To complete the solution, Eq. (4) is discretized and solved along with this equation to obtain the distribution of $\partial\Phi/\partial n$ and Φ_0.

With $\partial\Phi/\partial n$ known, the electric pressure $[=-\varepsilon_0(\boldsymbol{n} \cdot \nabla\Phi)^2/2]$ is readily obtained, and thus the droplet shapes may be calculated.[13] To simplify the computations, the hydrodynamic pressure and viscous contribution to the shape deformation is neglected. Thus for the cases considered in this study, the surface shapes are determined primarily by the balance between the surface tension and electrostatic forces. To facilitate the calculations, the normal stress balance equation is more conveniently written in a spherical coordinate system and solved using the weighted residuals method (WRM). To derive the formulation, the surface of the droplet is discretized and defined by R_i, the distance between the surface node and the center of the droplet. Following the procedure of the WRM,[13] one has the final equation for the surface coordinates R (Ref. 13):

$$\int_0^\pi \left\{ \frac{RR_\theta(\mathrm{d}\psi_i/\mathrm{d}\theta) + \psi_i\left(2R^2 + R_\theta^2\right)}{\sqrt{R^2 + R_\theta^2}} + R^2\psi_i\left(K + BR\cos\theta - \frac{a_d\varepsilon_0(\boldsymbol{n} \cdot \nabla\Phi)^2}{2\gamma}\right)\right\} \sin\theta \, \mathrm{d}\theta = 0 \tag{14}$$

The constraints of the volume conservation and the center of mass of the electrostatically levitated droplet are needed to determine the shape and position of the droplet:

$$\int_0^\pi R^3 \sin\theta \, \mathrm{d}\theta = 2 \tag{15}$$

$$\frac{3}{8}\int_0^\pi R^4 \cos\theta \sin\theta \, \mathrm{d}\theta = z_c \tag{16}$$

where z_c is the center of mass. The free surface may be discretized into N elements and Eqs. (14–16) are integrated numerically.[13]

With the surface shapes of the droplets known, the governing equations for the thermal and fluid flowfields along with the boundary conditions are solved using the Galerkin finite element method. To do that, the droplet is discretized into a group of elements, over each of which the dependent variables $\boldsymbol{u}$, P, and T are interpolated by the shape functions ϕ, ψ, and θ. Substituting the preceding equations into the governing equations and requiring that the residuals of the resultant equations be orthogonal to the shape functions, the Galerkin integral form of the governing equations for the fluid flow and heat transfer can be obtained as follows:

$$\left[\int_{\Omega_1} \psi\left(\hat{j} \cdot \nabla\phi^T + \delta_{2j}\phi^T \mid r\right) \mathrm{d}V\right] \boldsymbol{U}_j = -\varepsilon\left(\int_{\Omega_1} \psi\psi^T \, \mathrm{d}V\right)\boldsymbol{P} \tag{17}$$

$$\left(\int_{\Omega_1} \rho\phi\phi^T \, \mathrm{d}V\right)\frac{\mathrm{d}\boldsymbol{U}_i}{\mathrm{d}t} + \left(\int_{\Omega_1} \rho\phi\boldsymbol{u} \cdot \nabla\phi^T \, \mathrm{d}V\right)\boldsymbol{U}_i - \left[\int_{\Omega_1} (\hat{i} \cdot \nabla\phi + \delta_{2i}\phi/r)\psi^T \, \mathrm{d}V\right]\boldsymbol{P} + \left[\int_{\Omega_1} \eta\left(\nabla\phi \cdot \nabla\phi^T + 2\delta_{2i}\phi \cdot \phi^T \mid r^2\right) \mathrm{d}V\right]\boldsymbol{U}_i + \left[\int_{\Omega_1} \eta(\hat{i} \cdot \nabla\phi)(\hat{j} \cdot \nabla\phi^T) \, \mathrm{d}V\right]\boldsymbol{U}_j + \left(\int_{\Omega_1} \rho\beta\phi\theta^T\boldsymbol{g}\right)\boldsymbol{T} = \int_{\partial\Omega_1} \boldsymbol{n} \cdot \bar{\sigma} \cdot \hat{i}\phi \, \mathrm{d}s \tag{18}$$

$$\left(\int_{\Omega_1} \rho C_p \varphi\varphi^T \, \mathrm{d}V\right)\frac{\mathrm{d}\boldsymbol{T}}{\mathrm{d}t} + \left(\int_{\Omega_1} \rho C_p \varphi\boldsymbol{u} \cdot \nabla\varphi^T \, \mathrm{d}V\right)\boldsymbol{T} + \left(\int_{\Omega_1} k\nabla\varphi \cdot \nabla\varphi^T \, \mathrm{d}V\right)\boldsymbol{T} = -\int_{\partial\Omega_1} q_T\varphi \, \mathrm{d}s \tag{19}$$

Once the form of shape functions ϕ, φ, and ψ is specified, these equations can be integrated numerically. The resultant matrix equation is solved using the successive substitution method and the time derivatives are approximated using the implicit finite difference scheme.

The computational procedure for the calculation of the electric potential, free surface shapes, and thermal and fluid flowfields is outlined next. The calculation starts with an initial guess of a droplet shape, followed by the solution of the electric potential and electric pressure by the boundary element method and the free surface shape. The electric potential is then updated with the calculated shape and is used again to update the free surface shape for the next round calculation. The iteration continues until a convergence is achieved. With the free surface shapes so determined, the fluid flow and temperature distribution is calculated using the Galerkin finite element method as described earlier. The computer programs developed for these calculations have been checked against available analytical and numerical solutions. For all of the test cases, the match was within the machine accuracy.[5,13–15]

IV. Results and Discussion

The computational methodology described is capable of predicting the electric field distribution, electric pressure distribution along the surface of a droplet, droplet shapes, temperature distribution, and internal convection in the droplets driven by buoyancy and surface tension forces. Extensive numerical simulations were carried out. A selection of computed results is presented. In the present work, we focus on the behavior of a silicon droplet with various heating arrangements. Silicon was chosen because of its importance to the electronic industry and because it is one of the core materials being considered for microgravity experiments. Unless indicated otherwise, the computations were based on the physical properties and parameters listed in Table 1. Figure 2 shows the boundary element (heavy dots) and finite element meshes used for the computation.

Table 1 Parameters used in calculations

Si property	Value
T_{melt}, K	1685
Q_0, W/m^2	1.5×10^6
a_d, mm	2.5
ρ, kg/m^3	2510
μ, kg/m-s	0.94×10^{-3}
γ, N/m	0.864
$d\gamma/dT$, N/m-K	-1.3×10^{-4}
k, W/m-K	138.5
C_p, J/kg-K	1040
E, V/m	2.5×10^6
Emissivity ε_0	0.3
β, K^{-1}	7.6×10^{-6}
Pr	0.706×10^{-2}

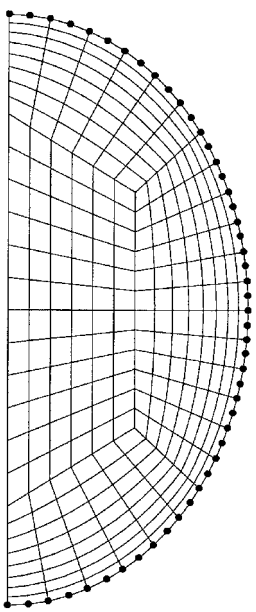

Fig. 2 Finite element mesh and boundary-element discretization for numerical computations.

A total of 48 linear boundary elements was used for the electric field calculations, and 24 quadratic boundary elements for the free surface computations. The thermal and flow calculations used 264 nine-node elements, with penalty formulation for pressure. A convergence criterion of 1×10^{-4} was set for relative error associated with all unknowns whenever an iterative procedure was applied. To determine the grid effect, different meshes and/or mesh distributions were used. The final mesh, as shown in Fig. 2, was chosen based on the criterion that any further refinement of mesh produces an error of less than 0.1% (relative to the final mesh).

To assess accurately the hydrodynamic pressure and viscous effects on the drop surface deformation, we also carried out the calculations of drop shapes with a full integration of thermal and fluid flowfields and electric field. These fully coupled calculations involved one additional iterative procedure that required updating of hydrodynamic pressure and normal viscous stresses in the free surface calculations and iterating among the electric, mechanical, and free surface variables. The integrated calculations, when converged, gave simultaneously the results of drop shapes, temperature and velocity fields, and electric stresses along the free surface. Calculated results for selected cases showed that the dynamic pressure and viscous stresses together contribute less than 2% for the worst-scenario case, but the inclusion of them increases the computational time substantially because the fluid flow computation now has to be included in the free-surface/electric-field iteration loop. Additional numerical simulations indicated that, for dynamic pressure and viscous stresses to produce more than 10% derivation in shape deformations, the drop must be heated to a very high temperature, typically within a few degrees (K) to the vaporization point. These suggest that, for applications considered for electrostatic levitation, drop deformation is essentially defined by the force balance between the electric and the surface tension forces along the free surface and that the hydrodynamic pressure and viscous stresses can be neglected to simplify the calculations. This is the approach taken in this paper.

A. Droplet Shapes

In microgravity, the electric forces are designed to position the droplet in a designated location. As a net lifting force is not needed, the total net charge is equal to zero. However, as the droplet is placed in the electric field, the electric field is perturbed and induces surface charges on the droplet. These induced surface charges interact with the imposed electric field to ensure that the electric field inside the droplet is zero or the entire droplet is at a constant potential. While the net force is zero, the local electric force along the surface is not zero, which must be balanced by the surface tension force, thereby defining a free surface profile for the droplet. Because the surface charges are negative on the lower half-surface and positive on the upper half-surface, they combine with an upward electric field to produce a force that pulls the surface away from the center. Moreover, the surface charges are symmetrically distributed due to the symmetry of the applied electric field. Consequently, the droplet deforms symmetrically and is pulled outward from the center.

Under terrestrial conditions, on the other hand, the positive charges interact with the imposed field to produce a net electric force, which acts to balance the gravitational force so as to keep the droplet levitated in air. For an electrically conducting sphere, the resulting local surface charges are a sum of the induced electric and the imposed charges and are nonuniformly distributed along the droplet surface. These charges interact with the electric field to produce an electric stress, which is then balanced by the mechanical stress resulting from gravity effects and surface tension. The equilibrium droplet shape in this case is plotted in Fig. 3. Clearly it is different from that of microgravity conditions in that the droplet shape is no longer symmetric, as the lower half is flatter than the upper half of the surface. Further calculations illustrate that an increase in the applied electric field, or the density of surface charges for the terrestrial case, causes greater surface deformation.

B. Thermal and Flowfields

As stated before, for an electrically conducting melt, the Maxwell stress is normal to the surface and thus no tangential shear stress

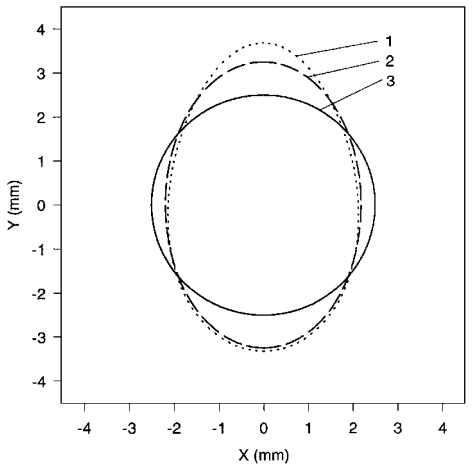

Fig. 3 Comparison of free surface profiles of a Cu droplet in normal and microgravity: 1, $E_0 = 3.3 \times 10^6$ V/m and $Q = 1.56 \times 10^{-9}$ C (normal gravity); 2, $E = 3.3 \times 10^6$ V/m and $Q = 0$ C (microgravity gravity); and 3, undeformed liquid sphere.

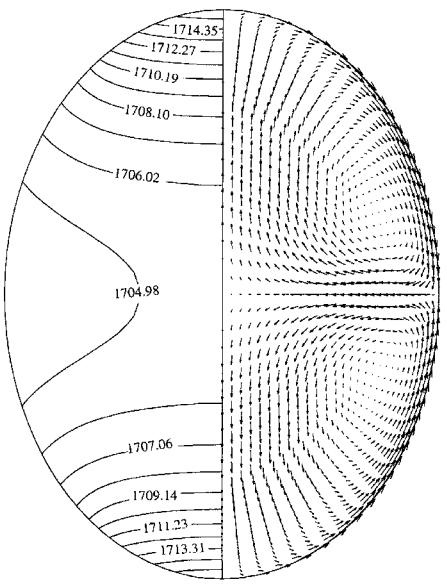

Fig. 4 Temperature distribution and internal velocity field in a Si droplet with heating at the two poles ($a_l = 1.25$ mm, $Q_0 = 1.5$ mW/m^2) in microgravity: $V_{max} = 13.1$ cm/s.

components exist. Because this stress field is nonvortical in nature, it generates no fluid motion in the droplet.[6] However, internal convection in a droplet electrostatically positioned in microgravity occurs when the surface tension varies as a function of temperature along the droplet surface. Three laser beam heating arrangements that are being considered at present are analyzed in this study: 1) heating at the two poles, 2) heating at one of the poles, and 3) heating around the equator by a ring source.

1. *Case 1: Heating at the Two Poles*

In this case the laser beams are applied to heat the regions around the two poles. The heating is symmetric with respect to the equatorial plane, and the laser beams themselves are of rotational symmetry with respect to the vertical axis, as shown in Fig. 1b. Because of the laser heating, a nonuniform temperature distribution arises in the droplet, which in turn induces the Marangoni convection. Figure 4 illustrates the thermal and fluid flowfields in the droplet when it is heated to a designated temperature, assuming that a steady state is achieved. The temperature contour clearly indicates that thermal transport within the droplet is affected by convection at this flow level. There exists a temperature difference of about 10 K in the droplet, with the maximum temperatures at the two poles and the minimum at the equator. This temperature difference produces a recirculating Marangoni convection in the droplet such that the fluid particle moves from the high-temperature region to the lower-temperature region on the surface and inside the droplet from the equator toward the pole regions. This recirculating Marangoni convection may be readily explained. As the surface tension of Si decreases with increasing temperature, a higher surface tension exists near the relatively cool equator. The higher surface tension exerts a greater pulling force on a fluid element on the surface and thus pulls the fluid element toward that region from the lower-surface tension (or higher-temperature) part of the surface. To satisfy the flow continuity, the mass within the Si droplet moves up from the equator to the pole regions, thereby forming an internal recirculating flow pattern.

In practice, when levitation is stabilized and the sample is heated to a designated temperature, the laser beam is turned off and the sample is allowed to cool below its melting point by exchanging energy with the environment. During this period, both fluid flow and temperature distribution are evolving. The computational methodology discussed here may also be applied to predict the dynamic development of these transient fields.

Figure 5 illustrates a set of snapshots of the time-evolving velocity and temperature fields in a Si droplet after the laser power is switched off and the droplet is allowed to cool to approximately 200 K below the melting point. The calculations began with the initial velocity and temperature fields as shown in Fig. 4. This set of results indicates that the radiative loss of heat to the surroundings results in a lower temperature at the poles and a higher temperature at the center of the sphere. A temperature gradient is also established such that the temperature at the equator is now higher than that at the two poles. This dynamic change in temperature results in the evolution of the fluid flowfield in the droplet. The internal flow reverses its rotating direction at some point in time after cooling takes place, and at this point two competing recirculating loops occur. The outer loop originates from the fact that the temperature at the pool cools below that at the equator plane and hence the surface tension forces tend to drive the fluid particles from the equator to the poles along the surface of the droplet. The inner loop, on the other hand, is a carryover from the initial flowfield and becomes weaker as cooling continues. Eventually, the inner loop is engulfed by the outer loop entirely.

Both transient and steady-state calculations were carried out for the electrostatically levitated Si droplets heated with the same heating source under terrestrial conditions. The recirculating flow patterns and thermal decay behavior are very similar to those described, indicating that the buoyancy effects are negligible in comparison with the surface tension effects for these droplets. Numerical results show further that the internal recirculating pattern and thermal decay behavior remain basically constant as laser heating area a_l is changed. However, the velocity level (or maximum velocity) is a strong of function of the laser heating area in that a smaller temperature gradient and hence a lower maximum velocity result from a larger area covered by the laser heating beam. The computed results for different-sized beams are given in Table 2 for both terrestrial and microgravity conditions.

2. *Case 2: Heating at One of the Poles*

This heating configuration is similar to case 1 but with only one laser beam directed at the sample. A situation like this can occur when additional instruments are mounted to obtain certain information on the droplets. The steady-state thermal and fluid flowfields for this case are given in Fig. 6, and those when the droplet undergoes cooling are plotted in Fig. 7. The temperature contour and fluid flow recirculating pattern differ from that described earlier. In the present case, there exists only one large toroidal velocity loop recirculating in half of the droplet, with the rotational axis defined by the axial axis of the laser beam. Both the maximum velocity and the temperature difference (i.e., between the maximum and the minimum temperatures) are higher. The thermal contour is also remarkably different in that the highest temperature occurs at the point facing the laser beam and the lowest at the opposite point along the rotational axis.

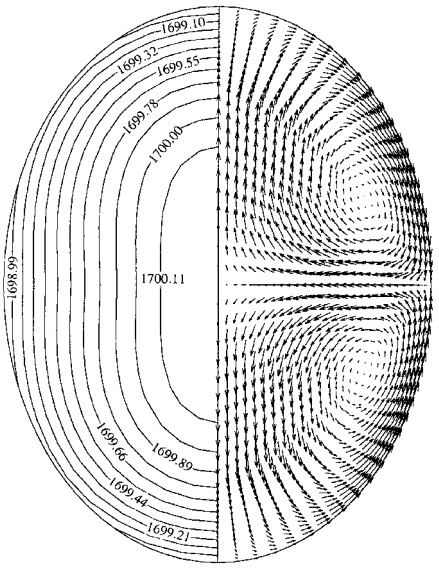

V_{max} = 44.5 cm/s; time = 0.1 s

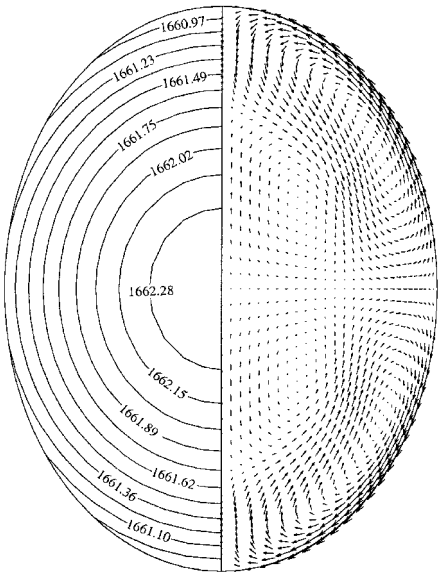

V_{max} = 7.81 cm/s; time = 0.7 s

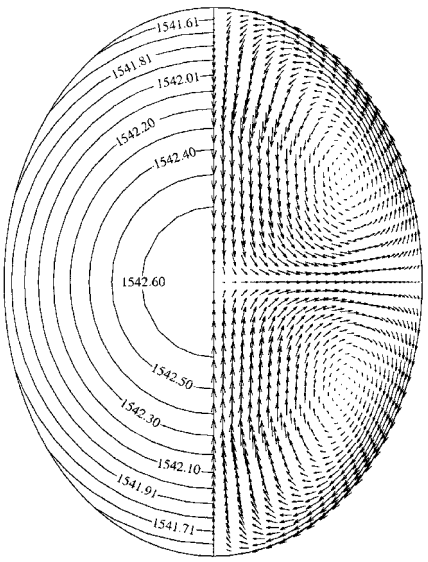

V_{max} = 1.06 cm/s; time = 3 s

Fig. 5 Dynamic development of temperature and internal convection fields in a Si droplet as it undergoes cooling in microgravity with heating at the two poles.

Table 2 Effects of heat source arrangements on temperature difference and maximum velocity in an electrostatically levitated silicon droplet

Case	a_l, mm	Q_0, mW/m^2	T_{avr}, K	ΔT, K	U_{max}, cm/s
		g = 0			
Symmetric	0.75	5.2	1703.7	22.3	21.22
heating at	1.25	1.5	1709.7	11.5	13.1
two poles	1.85	0.65	1719.0	6.6	10.03
	2.276	0.27	1694.1	1.8	3.6
Asymmetric	0.75	10.5	1717.0	46.7	32.38
heating at	1.25	3.0	1713.4	25.7	21.8
one pole	1.85	1.25	1704.0	16.8	17.67
	2.276	0.55	1709.7	10.5	13.4
Ring heat	0.75	0.66	1695.0	5.5	9.91
source	1.25	0.43	1704.2	4.6	8.78
	2.25	0.25	1705.0	3.1	6.51
	3.011	0.19	1708.3	1.4	3.28
		g = 9.81, m/s^2			
Symmetric	0.75	5.2	1705.4	22.74	21.18
heating at	1.25	1.5	1722.5	12.0	13.3
two poles	1.85	0.65	1720.3	6.8	10.09
	2.273	0.27	1700.1	1.7	3.5
Asymmetric	0.75	10.5	1722.2	47.57	32.43
heating at	1.25	3.0	1718.6	26.3	21.9
one pole	1.85	1.2	1708.0	17.12	17.85
	2.273	0.55	1714.3	10.5	13.4
Ring heat	0.75	0.66	1693.4	5.5	9.91
Source	1.25	0.43	1703.2	4.7	8.82
	2.25	0.25	1704.3	3.13	6.54
	3.043	0.18	1687.0	1.3	3.12

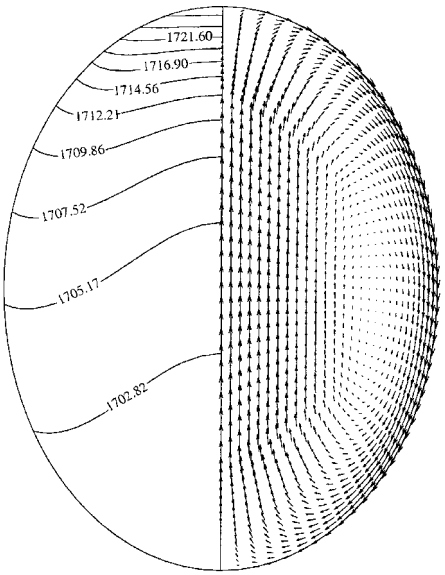

Fig. 6 Temperature distribution and internal velocity field in a Si droplet with heating at one of the two poles (a_l = 1.25 mm, Q_0 = 3.0 mW/m^2) in microgravity: V_{max} = 21.8 cm/s.

As one might expect, the timely change of the velocity and temperature fields is also different in the droplet when the laser beam is shut off to allow the droplet to cool into the undercooling region. Initially, the single flow loop occupies the entire droplet. As time goes by, a second loop starts to appear near the north pole and gradually evolves and enlarges in size until it occupies the whole upper half of the droplet. This change in flow structure is accompanied by the temperature change, which gradually evolves into a symmetric pattern with the temperature highest at the equator and decreasing toward the two poles, as appears in Fig. 7.

Calculations were also carried out for terrestrial conditions and for different heating sources. As in the case of the symmetric heating (or heating at the two poles), buoyancy effects play a minor role,

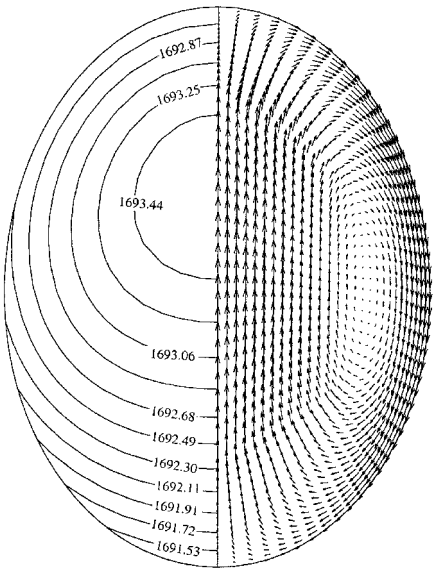

V_{max} = 8.70 cm/s; time = 0.2 s

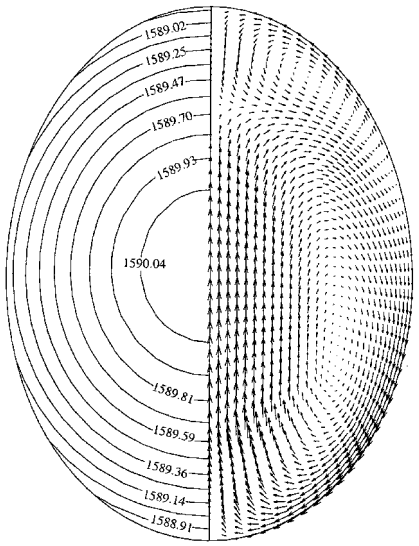

V_{max} = 1.23 cm/s; time = 2 s

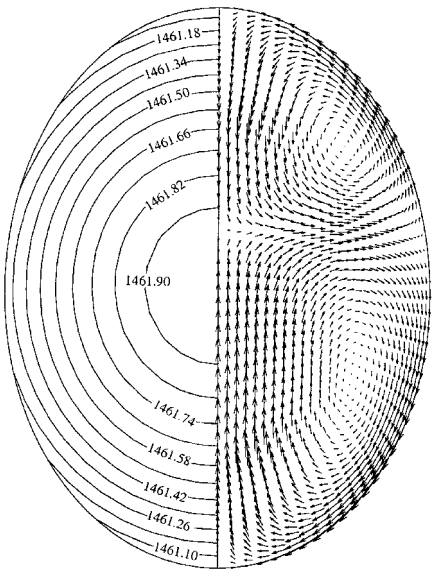

V_{max} = 0.9 cm/s; time = 5 s

Fig. 7 Dynamic development of temperature and internal convection fields in a Si droplet as it undergoes cooling in microgravity with heating at one of the two poles.

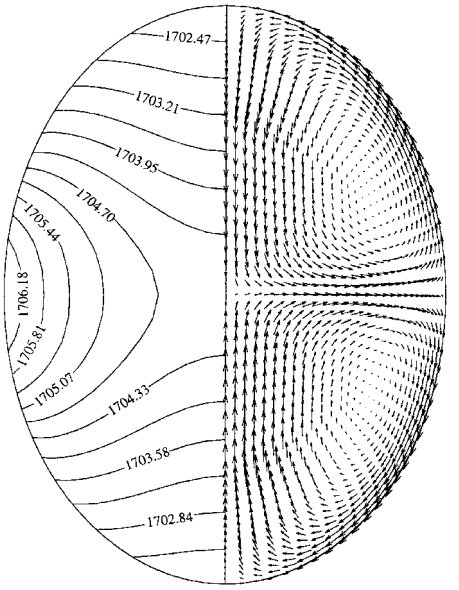

Fig. 8 Temperature distribution and internal velocity field in a Si droplet with a heat ring source around the equator (a_l = 1.25 mm, Q_0 = 0.43 mW/m^2) in microgravity: V_{max} = 8.78 cm/s.

and a larger laser beam coverage results in a reduction of velocity intensity in the droplet, as is evident from Table 2. Also, the evolution of fluid flow and thermal fields inside the droplet follows very similar patterns, as shown in Fig. 7.

3. *Case 3: Heat Ring Source Around the Equator*

In this heating configuration, a ring heat source is located around the equator of the droplet. The steady-state thermal and fluid flowfields for this case are given in Fig. 8. It is noted that, for this type of heating, the flow recirculates in the opposite direction as shown in Fig. 4 and the fluid particles on the droplet surface move from the equator to the two poles. This is readily explained by the fact that, for this type of heating, the higher temperature occurs at the equator plane and temperatures are lower near the two poles. Unlike the preceding two cases, the temperature contour remains the same, with the higher temperature remaining at the equator plane, after the laser beam is switched off. Because of this, the fluid flow recirculating pattern also remains the same. However, the magnitude of both temperature and velocity in the droplet becomes diminished as cooling continues. Calculations were also carried out for terrestrial conditions and for various heating areas defined by a_l. The results are given in Table 2. Again, the natural convection effects are minimum and contribute at most about a 5% difference. Also, the larger laser beam coverage results in a lower velocity and a more uniform temperature distribution in the droplet. Furthermore, inspection of the results in Table 2 also indicates that a ring heat source is preferable, if the instrument arrangement allows, as the convection and thermal nonuniformity are much reduced in comparison with two other cases. Care, however, has to be exercised to position the drop at the center of the heating source, because any perturbations would cause deleterious unsteady flows. In this regard, a microgravity environment can be particularly useful in that only a minuscule electric force is required to control the drop in position.

It is noteworthy that hydrodynamic instability in thermocapillary flows may occur under certain conditions, and its occurrence destroys the symmetric steady-state flow structure, thereby leading to oscillatory or three-dimensional flows.[16,17] The phenomena have been analyzed for other configurations. On the basis of the criteria published, all of the cases presented are estimated well within the stable regime. Of course, detailed study is required to establish a precise criterion for levitated drops, which is beyond the scope of this work. Nonetheless, the computational methodology and results presented should serve well as a basis on which instability studies on drops are carried out.

V. Conclusion

A numerical study of surface deformation, Marangoni convection, and temperature distribution in an electrostatically levitated melt droplet under both terrestrial and microgravity conditions has been presented. In developing the numerical model for the study, the boundary element method was applied to obtained the solution of the electric field distribution outside the droplet. The equilibrium droplet shapes are defined by the normal stress balance equation involving electrostatic stresses, surface tension, and hydrostatic pressure when gravity is present. The equation was solved using the weighted residuals method. The internal fluid flow and temperature distribution in the electrostatically deformed droplet were calculated using the finite element method. Numerical simulations were carried out for the effects of different heat source arrangements on the thermal and fluid flow behavior of the droplet. The results show that the droplet deforms into an ellipsoidal shape under the pulling action of the electrostatic normal stresses induced by the applied electric field. A noticeable Marangoni convection can occur for all of the laser heat source arrangements. Among the three arrangements examined, a ring heat source gives rise to the lowest velocity level and temperature gradient, whereas the largest velocity and temperature difference occur when heating is applied at only one of the poles. For all of the cases, a larger laser beam coverage results in a reduction of the temperature difference and thermally induced flows in the droplet. To eliminate completely the convection in the droplet, a uniform heat source needs to be applied. The computational methodology presented should be very useful in exploring various heat source designs for electrostatic levitation applications.

Acknowledgment

Financial support of this work by the NASA Microgravity Science and Applications Division (Grant NAG8-1477) is gratefully acknowledged.

References

[1]Rhim, W. K., Chung, S. K., and Barber, D., "An Electrostatic Levitator for High Temperature Containerless Materials Processing in 1-g," *Review of Scientific Instruments*, Vol. 64, No. 10, 1993, pp. 2961–2970.

[2]Rhim, W. K., "Thermophysical Property Measurements of Molten Semiconductors," *NASA Microgravity Materials Science Conference*, edited by F. Szofran, D. McCauley, and C. Walker, NASA Conf. Publication 3342, 1997, pp. 427–432.

[3]Zong, J.-H., Li, B. Q., and Szekely, J., "The Electrodynamic and Hydrodynamic Phenomena in Magnetically-Levitated Droplets, Part I. Steady State Behavior," *Acta Astronautica*, Vol. 26, No. 6, 1992, pp. 435–449.

[4]Zong, J. H., Li, B. Q., and Szekely, J., "Electrodynamic and Hydrodynamic Phenomena in Magnetically-Levitated Molten Droplets: Transient Behavior and Heat Transfer Considerations," *Acta Astronautica*, Vol. 29, No. 4, 1993, pp. 305–311.

[5]Song, S. P., and Li, B. Q., "A Boundary/Finite Element Analysis of Magnetic Levitation Systems: Surface Deformation and Thermal Phenomena," *Journal of Heat Transfer*, Vol. 120, No. 2, 1998, pp. 492–504.

[6]Taylor, G. I., "Studies in Electrodynamics," *Proceedings of the Royal Society of London*, Vol. 291, 1966, pp. 159–166.

[7]Adornato, P. M., and Brown, R. A., "Shape and Stability of Electrostatically Levitated Drops," *Proceedings of the Royal Society of London, Series A: Mathematical and Physical Sciences*, Vol. 389, No. 1796, 1983, pp. 101–117.

[8]Feng, J. Q., and Beard, K. V., "Small-Amplitude Oscillations of Electrostatically Levitated Drops," *Proceedings of the Royal Society of London, Series A: Mathematical and Physical Sciences*, Vol. 430, No. 1878, 1990, pp. 133–154.

[9]Sadhal, S. S., Trinh, E. H., and Wagner, P., "Thermocapillary Flows in a Drop with Unsteady Spot Heating in a Microgravity Environment," *Microgravity Science and Technology*, Vol. 9, No. 2, 1996, pp. 80–86.

[10]Li, B. Q., and Song, S. P., "Surface Oscillation and Fluid Flow in Magnetically-Positioned Droplets Under Microgravity Conditions," *Japanese Journal of Microgravity Science*, Vol. 15, 1998, pp. 331–336.

[11]Jackson, J. D., *Classical Electrodynamics*, Wiley, New York, 1976.

[12]Song, S. P., and Li, B. Q., "Coupled Boundary and Finite Element Computation of Magnetically-Levitated Droplet Shapes," *Boundary Element Technology XII*, edited by J. I. Frankel, C. A. Brebbia, and M. A. H. Aliabadi, Wessex Inst. of Technology, Southampton, England, U.K., 1997, pp. 239–250.

[13]Song, S. P., and Li, B. Q., "A Coupled Boundary/Finite Element Method for the Computation of Magnetically- and Electrostatically-Levitated Droplet Shapes," *International Journal for Numerical Methods in Engineering*, Vol. 44, 1999, pp. 1055–1077.

[14]Song, S. P., Li, B. Q., and Khodadadi, J. A., "Coupled Boundary/Finite Element Solution of Magnetothermal Problems," *International Journal of Numerical Methods for Heat and Fluid Flow*, Vol. 8, No. 3, 1998, pp. 321–349.

[15]Pan, B., Li, B. Q., and de Groh, H. C., "Magnetic Damping of g-Jitter Induced Flow in Microgravity," *Spacebound-97: Experimental Methods for Microgravity Materials Science*, edited by J. Sygusch, Canadian Space Agency, Montreal, QC, Canada, 1997, pp. 347–360.

[16]Wanschura, M., Shevtsova, V. M., and Rath, H. J., "Convective Instability Mechanisms in Thermocapillary Liquid Bridges," *Physics of Fluids*, Vol. 7, 1995, pp. 912–918.

[17]Davis, S., "Thermocapillary Instabilities," *Annual Review of Fluid Mechanics*, Vol. 19, 1987, pp. 403–435.